International Journal of Minerals, Metallurgy and Materials
Volume 27, Number 3, March 2020, Page 362
https://doi.org/10.1007/s12613-019-1894-6

Machine-learning-assisted prediction of the mechanical properties of Cu–Al alloy

Zheng-hua Deng[1,2], *Hai-qing Yin*[1,3], *Xue Jiang*[1,3], *Cong Zhang*[1,3], *Guo-fei Zhang*[1], *Bin Xu*[1],
Guo-qiang Yang[1], *Tong Zhang*[4], *Mao Wu*[4], *and Xuan-hui Qu*[1,4]

1) Collaborative Innovation Center of Steel Technology, University of Science and Technology Beijing, Beijing 100083, China
2) Chongqing Engineering Technology Research Center for Light Alloy and Processing, Chongqing Three Gorges University, Chongqing 404000, China
3) Beijing Advanced Innovation Center for Materials Genome Engineering, Beijing 100083, China
4) Institute for Advanced Materials and Technology, University of Science and Technology Beijing, Beijing 100083, China

(Received: 1 July 2019; revised: 2 August 2019; accepted: 16 August 2019)

Abstract: The machine-learning approach was investigated to predict the mechanical properties of Cu–Al alloys manufactured using the powder metallurgy technique to increase the rate of fabrication and characterization of new materials and provide physical insights into their properties. Six algorithms were used to construct the prediction models, with chemical composition and porosity of the compacts chosen as the descriptors. The results show that the sequential minimal optimization algorithm for support vector regression with a puk kernel (SMOreg/puk) model demonstrated the best prediction ability. Specifically, its predictions exhibited the highest correlation coefficient and lowest error among the predictions of the six models. The SMOreg/puk model was subsequently applied to predict the tensile strength and hardness of Cu–Al alloys and provide guidance for composition design to achieve the expected values. With the guidance of the SMOreg/puk model, Cu–12Al–6Ni alloy with a tensile strength (390 MPa) and hardness (HB 139) that reached the expected values was developed.

Keywords: powder metallurgy; tensile strength; hardness; machine learning; Cu–Al alloy; SMOreg/puk

1. Introduction

Copper alloys are widely used in pumps, bearings, propellers, engineering tools, dies, etc. [1–2], because of their high strength, hardness, wear resistance, and corrosion resistance. Tensile strength and hardness are the most important mechanical properties of aluminum bronze. At present, the mechanical properties of aluminum bronze are assessed using various destructive testing methods [3], which are both time-consuming and expensive. Therefore, an effective method for predicting the mechanical properties of aluminum bronze is urgently needed.

In recent years, machine learning has been widely used to predict the mechanical properties of materials. Altinkok and Koker [4] used the back-propagation artificial neural network (BP-ANN) model to successfully predict the bending strength and hardness of aluminum matrix composites. Zhao *et al*. [5] used the particle swarm optimization algorithm with back-propagation (PSOA-BP) model to predict the bending strength of Cu–Sn–Ti composites with high accuracy. Tang *et al*. [6] used support vector regression (SVR) to predict the strength of Al–Cu–Mg–Ag alloy. Compared with BP-ANN, the established SVR model was found to provide greater prediction accuracy under identical training. Liu *et al*. [7] developed a high-precision ANN model to predict the ultimate tensile strength of Nb–Si alloy. When they used the model to optimize the microstructure of a sample, its strength could reach the target value. Yang *et al*. [8] used the ANN model to predict the mechanical properties of A357 alloy, and their results showed that the BP model had high prediction accuracy. Razavi *et al*. [9] used the ANN model to predict the hardness of 17-4PH alloy and optimized a heat-treatment process to achieve the maximum hardness.

Notably, the literature contains few reports on predic-

Corresponding author: Hai-qing Yin E-mail: hqyin@ustb.edu.cn

tions of the mechanical properties of Cu–Al alloys. In the present study, six algorithms were used to model and predict the tensile strength and hardness of Cu–Al alloys. The model with the best performance was then used to guide chemical composition selection.

2. Modeling procedure

The process of building a machine-learning model can be divided into three stages: data collection, modeling, and model validation.

2.1. Data collection

Three constraints on the chemical elements and processing method were imposed in the data collection.

(1) The mass fraction of the additional alloying elements must be less than the mass fraction of Al.

(2) The preparation methods of the Cu–Al alloys were confined to casting and powder metallurgy to reduce the effect of processing on material properties.

(3) Because of the very limited amount of data for other elements, only conventional alloying elements such as Al, Fe, Ni, and Mn were used, which may adversely affect the accuracy of the data mining.

The chemical composition of a material is the most important factor governing its microstructure and properties [10]. Aluminum is a key alloying element, with its concentration in Cu–Al alloys ranging from 5wt% to 14wt%. When the Al content is less than 9.4wt%, the alloy contains only the α phase and exhibits low hardness and strength. When the Al content exceeds 9.4wt%, the alloy consists of both the α phase and the γ_2 phase and exhibits high hardness and low strength. The addition of other alloying elements such as Ni, Fe, and Mn can change the structure and properties of the alloy. Fe can refine grains and improve the mechanical properties, Ni can enlarge the α-phase region and refine grains, and Mn can reduce the eutectoid transformation temperature [11].

The porosity of a sintered compact strongly influences its mechanical properties. The occurrence of porosity reduces the tensile strength, and both ductility and fatigue resistance are highly sensitive to porosity [12]. The porosity of casting alloys is typically zero, whereas that of sintered compacts is greater than zero. Therefore, porosity is also used to distinguish between the two processes.

In the present study, the weight percentage of each element (Al, Fe, Ni, and Mn) and the porosity of the material were used as descriptors.

After the constraints and descriptors were applied, 142 items of experimental data were collected in a tensile-strength dataset and 100 items of experimental data were collected in a hardness dataset (these datasets were freely accessed at http://www.materdata.cn/search2.php?tty=798). The datasets were constructed using the results of laboratory experiments in the present study and those from the literature [13–40].

2.2. Modeling

Neutral networks and support vector machines (SVMs) have been widely used for data mining [41]. A neural network is a typical nonlinear and adaptive mathematical algorithm. It has shown good fitting prediction ability in certain cases where accurate descriptions are difficult to obtain with mathematical models [42]. However, a SVM can effectively solve the problem of high-dimensional data model construction under finite sample conditions and it has strong generalization ability [43].

In the present study, six machine-learning algorithms were considered to build a prediction model with the Weka software: standard linear regression (LR); multilayer perceptron or back-propagation neural network (MLP); sequential minimal optimization algorithm for support vector regression (SMOreg) with a poly kernel (SMOreg/poly), puk kernel (SMOreg/puk), or normalized poly kernel (SMOreg/norpoly); and support vector regression with a poly kernel (SVR/poly). To reduce the over-fitting in nonlinear regression, an n-fold cross validation was generally applied. In this work, a 5-fold cross validation was used. The dataset was divided into five nearly equal portions. Each portion was used once as the testing data. When a given portion of data represented the testing data, the other four portions were treated as the training data [44]. The final results were averages of the five test results.

Fig. 1 and Fig. 2 show the predicted values of tensile strength and hardness, respectively, plotted against the corresponding experimental data. The experimental and predicted values lie approximately on the $Y = X$ line, which demonstrates that the model accurately predicts the mechanical properties of the alloy. According to Fig. 1 and Fig. 2, the SMOreg/puk model showed the best fit at the training step.

The correlation coefficient (CC), mean absolute error (MAE), and root-mean-squared error (RMSE) were used to evaluate the performance of the prediction models based on the six algorithms [12,44].

Fig. 3 lists the values of CC, RMSE, and MAE for the six machine-learning models. The SMOreg/puk model shows the best performance, and its CC values for the tensile-strength model and hardness model are 0.9180 and 0.9373,

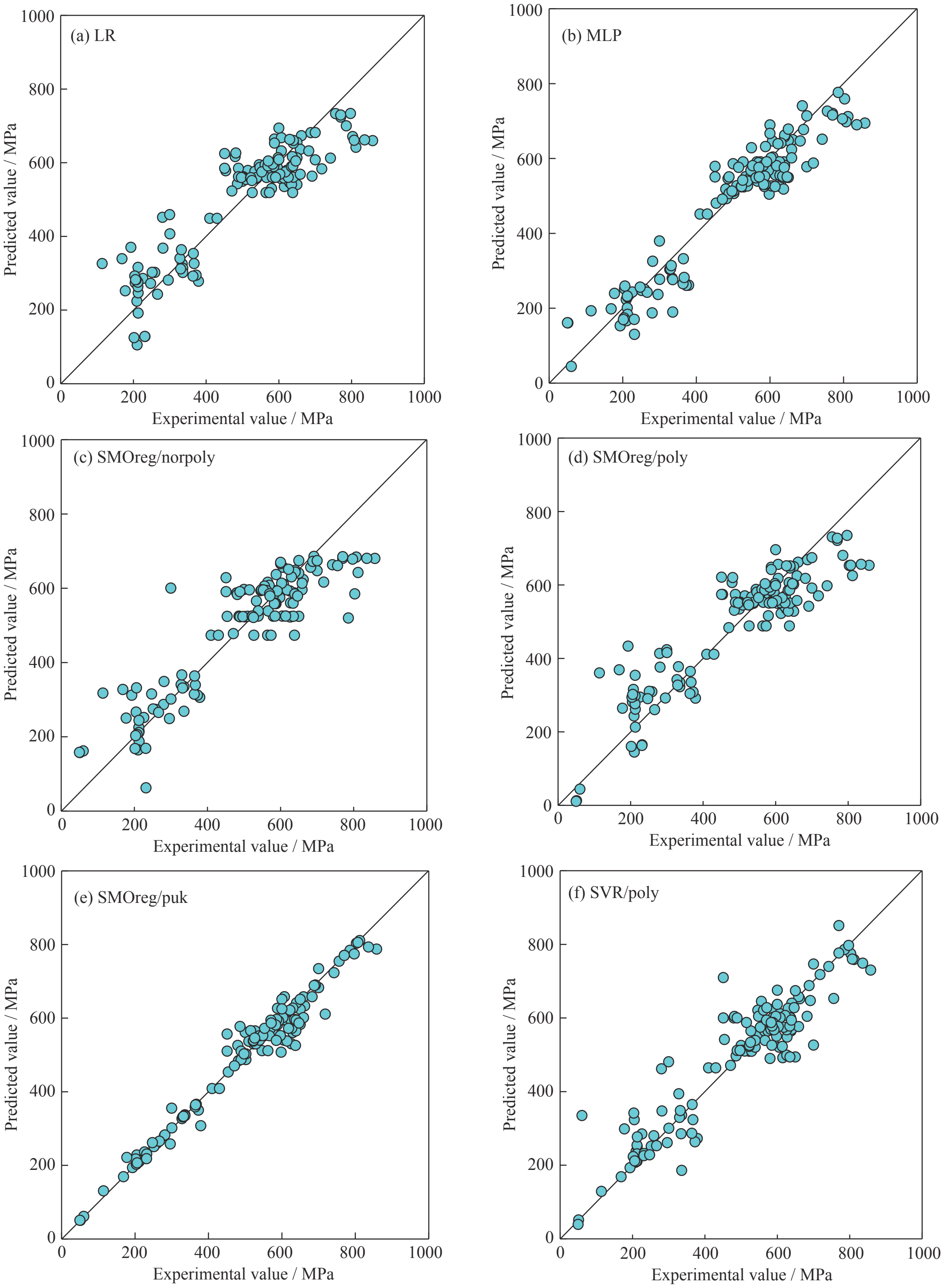

Fig. 1. Performance of machine-learning models on the training dataset to predict tensile strength: (a) LR; (b) MLP; (c) SMOreg/norpoly; (d) SMOreg/poly; (e) SMOreg/puk; (f) SVR/poly.

respectively. The MAE and RMSE values for the tensile strength predicted by the SMOreg/puk model are 52.1486 and 73.6705 MPa respectively, and the MAE and RMSE values for hardness predicted by the SMOreg/puk model are

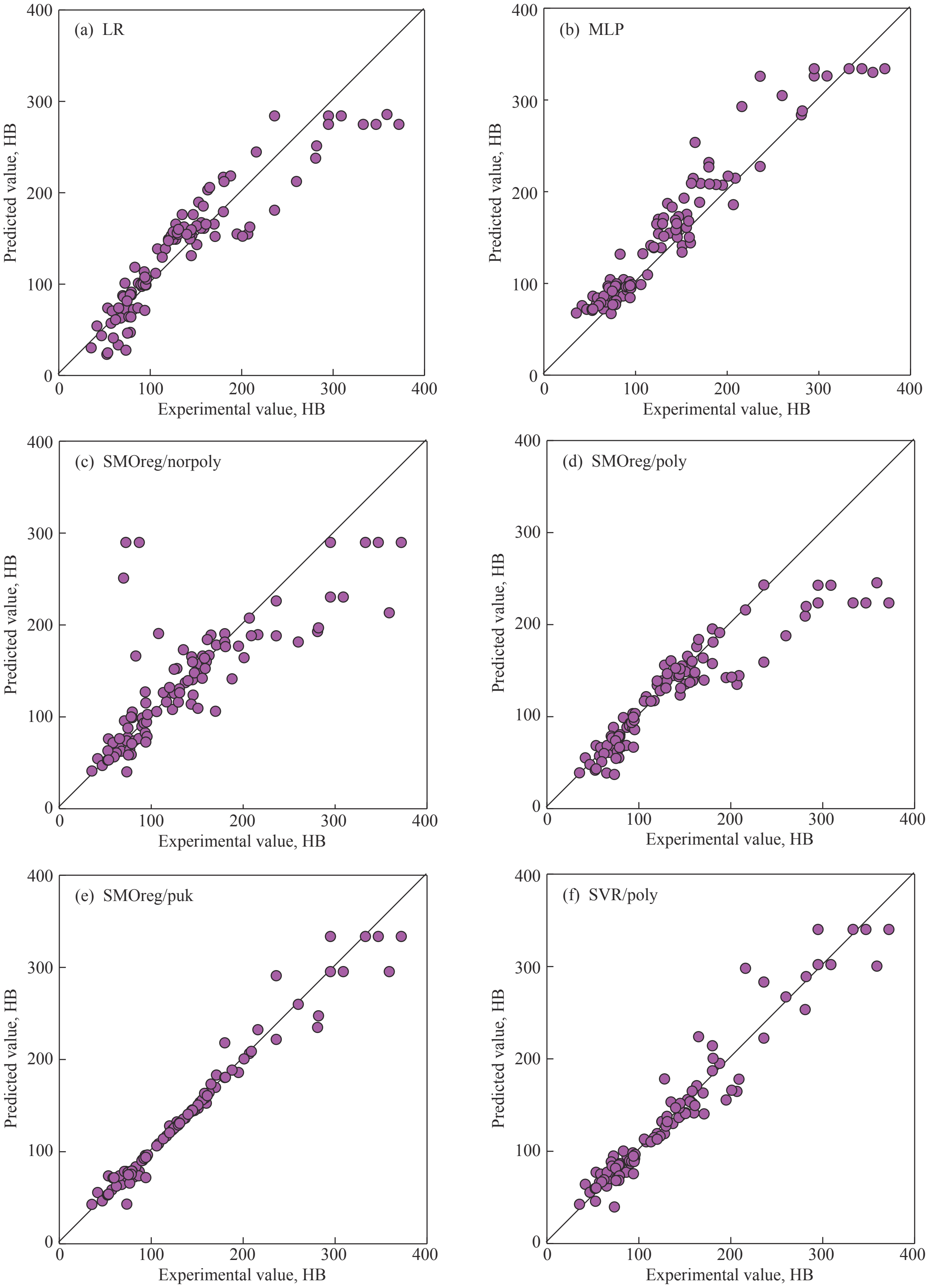

Fig. 2. Performance of machine-learning models on the training dataset to predict hardness: (a) LR; (b) MLP; (c) SMOreg/norpoly; (d) SMOreg/poly; (e) SMOreg/puk; (f) SVR/poly.

HB 16.9153 and HB 26.2977, respectively. These values are lower than those of the other models. Therefore, the SMOreg/puk model was selected for predicting the tensile strength and hardness.

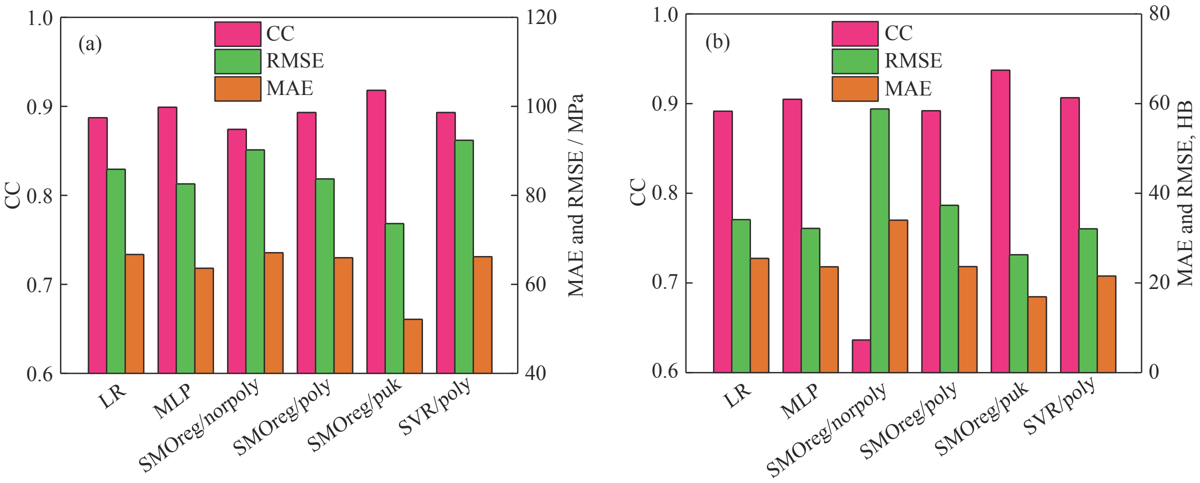

Fig. 3. CC, RMSE, and MAE of six machine-learning models applied to the training dataset: (a) tensile strength; (b) hardness.

2.3. Model validation

To validate the accuracy of the SMOreg/puk prediction model for tensile strength and hardness, we compared the predicted values with experimental values of the validation dataset (Fig. 4). The validation datasets were obtained both from experiments and the literature [39,45–47], and these data were not included in the training dataset above. The validation datasets are listed in Table 1. A comparison of the predicted and experimental values of tensile strength and hardness on the validation datasets reveals that the predicted values are consistent with the experimental ones. The maximum error of tensile strength is only 30.49 MPa (Fig. 4(a)), and the maximum error of hardness is only HB 8.6 (Fig. 4(b)).

3. Model application

The SMOreg/puk model was used to guide the composition design of the Cu–Al alloy such that its mechanical properties could reach the target values. The objective, a new high-strength Cu–Al matrix oil-bearing material with a porosity of approximately 11.5%, tensile strength greater than 350 MPa, and hardness of HB 135–140 was to obtain through composition design. The high-strength Cu–Al alloy in this case is intended for use as a bearing material with superior self-lubricating performance. The pores in the structure provide space for solid lubricants such as graphite and MoS_2 or a liquid lubricating oil.

The values predicted using SMOreg/puk model for the Cu–Al powder alloy were used to plot a distribution map of

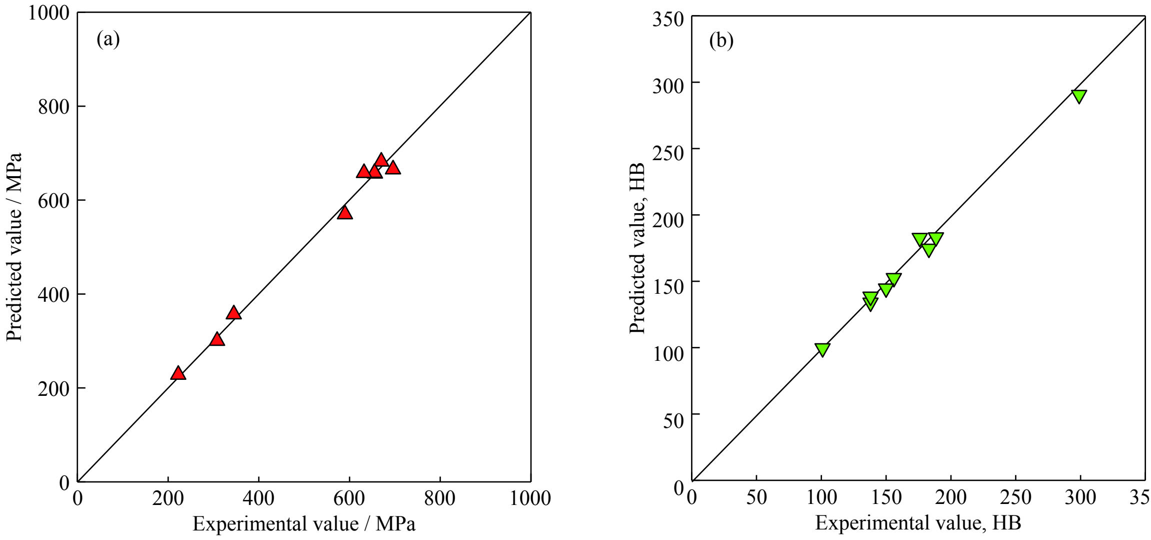

Fig. 4. Predicted tensile strength (a) and hardness values (b) of SMOreg/puk model on the validation dataset compared with the corresponding experimental values.

Table 1. Validation datasets of the SMOreg/puk prediction model

No.	Al / wt%	Ni / wt%	Fe / wt%	Mn / wt%	Porosity / %	Tensile strength / MPa	Hardness, HB	References
1	9.26	4.40	3.92	1.15	0.00	696.00	176.00	[45]
2	9.38	5.91	4.07	1.19	0.00	656.00	—	[45]
3	9.65	7.93	4.04	1.19	0.00	590.00	183.00	[45]
4	9.50	5.00	4.50	1.00	0.00	670.00	—	This work
5	9.00	4.50	4.00	1.15	0.00	655.00	188.50	This work
6	9.89	4.20	4.12	2.03	0.00	632.00	—	[46]
7	12.00	0.00	4.00	0.00	11.97	308.00	156.00	This work
8	12.00	0.00	0.00	5.00	10.70	345.00	150.00	This work
9	10.00	4.00	4.00	0.00	12.03	222.50	101.00	This work
10	9.72	0.00	0.91	0.00	0.00	—	138.00	[39]
11	14.00	0.35	3.00	1.25	0.00	—	299.00	[47]
12	12.00	6.00	5.00	0.00	11.55	—	138.00	This work

the tensile strength and hardness with the change of each descriptor, as shown in Fig. 5 and Fig. 6, respectively. The larger values in Fig. 5 and Fig. 6 are fitted by black curves. As shown in Fig. 5, when the porosity is approximately 11.5%, the tensile strength of the Cu–Al alloy reaches 350 MPa. When the Al content is 11.7wt%–12.2wt%, the tensile strength of the alloy reaches its highest value. When the Ni content is 6.0wt%–6.5wt%, the tensile strength of the alloy reaches its highest value. When the Mn content is 0wt% and 2.8wt%–3.2wt%, the strength of the alloy may reach its highest value. However, the tensile strength decreases with increasing Fe content.

As shown in Fig. 6, when the porosity is less than 13.0%, the hardness of the alloy reaches its target value. With increasing Al content, the hardness of the alloys gradually increases. When the Al content is greater than 11.2wt%, the hardness of the alloy reaches the target value. With increasing Ni or Mn content, the hardness decreases. When the Ni content is less than 6.6wt%, the hardness of the alloy reaches the target value. Within the range of known Mn content, the hardness of all of the alloys can reach the target value. However, as the Fe content increases, the hardness first increases and then decreases. When the Fe content is less than 3.8wt%, the hardness of the alloy can reach the target value. In this case, the content range of each element selected according to hardness includes the content range of each element selected according to tensile strength.

On the basis of the aforementioned results, the following composition ranges of various components were selected, and tensile strength and hardness were predicted using the SMOreg/puk model: 11.7wt%–12.2wt% Al, 6.0wt%–6.5wt% Ni, 0wt% Fe, and 0wt% or 2.8wt%–3.2wt% Mn, including Cu–(11.7–12.2)Al, Cu–(11.7–12.2)Al–(6.0–6.5)Ni, Cu–(11.7–12.2)Al–(6.0–6.5)Ni–(2.8–3.2)Mn, and Cu–(11.7–12.2)Al–(2.8–3.2)Mn. The step size for varying the chemical composition was set at 0.1wt%. Analysis of the prediction results revealed that when the chemical composition was close to Cu–12Al–6Ni, the mechanical properties of the alloy reached target values, with a tensile strength of 380 MPa and hardness of HB 138.

4. Experimental

The target porosity for the Cu–Al alloy was chosen as 11.5% according to the literature [12], and the process parameters for fabricating the alloy were selected as follows. Elemental powders of Cu, Al, and Ni produced by Xing Rong Yuan Co., Ltd. were used as the raw materials. The morphology and characteristics of the three elemental powders are shown in Fig. 7 and listed in Table 2, respectively. In Table 2, D_{10}, D_{50}, and D_{90} correspond to the point where the cumulative mass from the small-particle-diameter side reaches 10%, 50%, and 90% in the cumulative particle size distribution. Cu powder was mixed with 12wt% Al and 6wt% Ni in a tube mixer for 3 h. The mixed powder was compacted into 20-mm-diameter discs at 550 MPa. The green compact was heated to 1000°C for 1 h in a furnace under an H_2 atmosphere at a heating rate of 5°C/min, and then cooled in the furnace.

The microstructure of the samples was observed using a RX50M optical microscope and a JSM-7001F scanning electron microscope (SEM). The elemental distributions were analyzed by energy-dispersive spectroscopy (EDS) using a spectrometer installed on the scanning electron microscope. X-ray diffraction (XRD) analysis of the samples was performed using a Rigaku SmartLab X-ray diffractometer. The hardness was measured using a HB3000 Brinell hardness sclerometer, and the tensile strength was measured using an Instron 5569 universal testing machine.

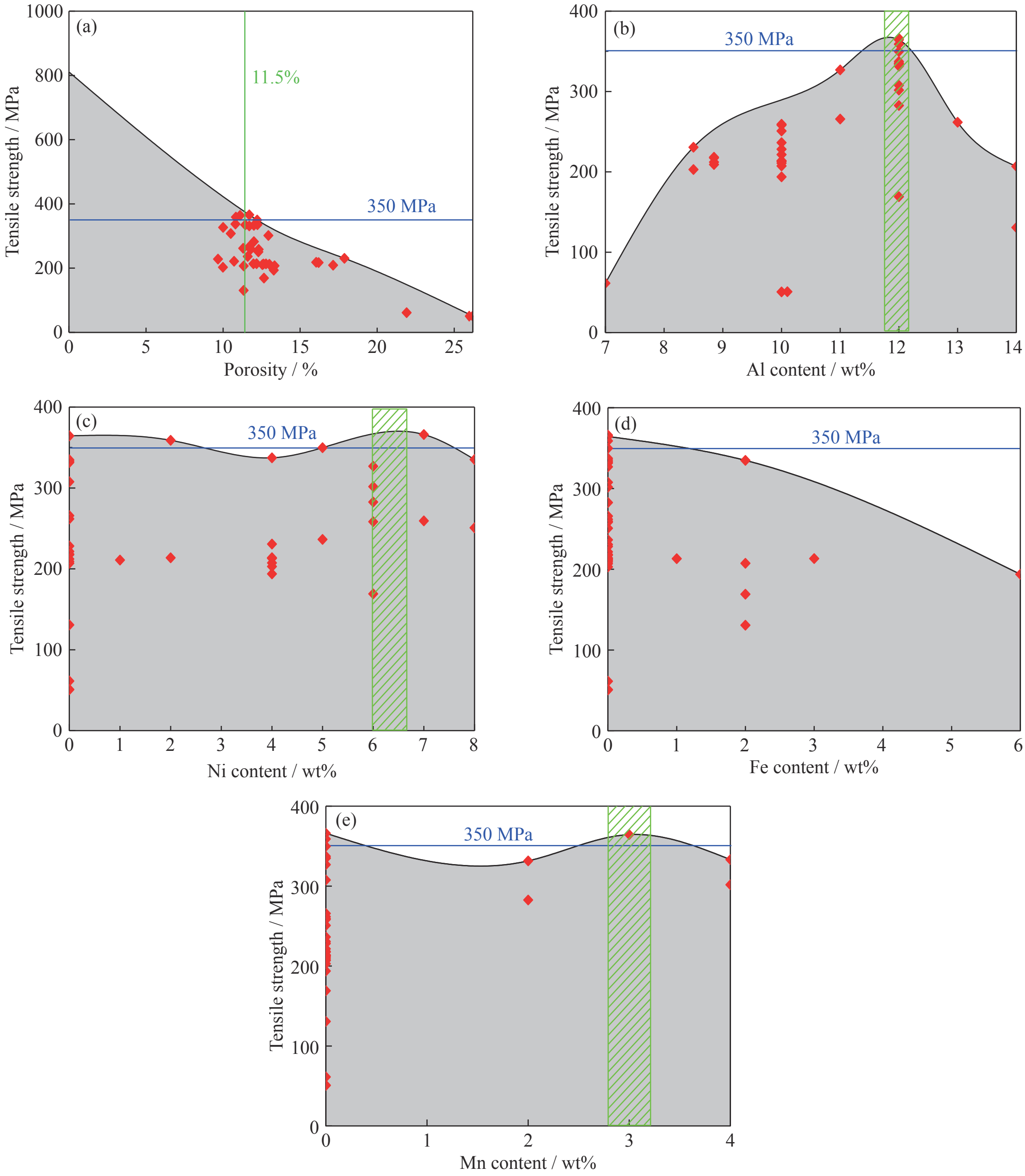

Fig. 5. Tensile-strength distribution of the alloy with respect to its porosity and composition obtained using SMOreg/puk model: (a) porosity; (b) Al content; (c) Ni content; (d) Fe content; (e) Mn content.

The sintered density (ρ_s) of the compacts was measured using Archimedes' law, and the porosity (ε) of the samples was calculated by the following Eq. (1) and Eq. (2) [48]:

$$\rho_a = 1/(x_1/\rho_1 + x_2/\rho_2 + \ldots + x_n/\rho_n) \tag{1}$$

$$\varepsilon = 1 - \rho_s/\rho_a \tag{2}$$

where ρ_a is the theoretical density of the alloy, ρ_n is the density of the nth element, and x_n is the mass fraction of the nth element.

5. Results and discussion

An optical micrograph of the Cu–12Al–6Ni alloy is presented in Fig. 8. The microstructure of all of the alloys consisted of α-Cu matrix phase (light-yellow regions), NiAl phase (dark-brown regions), and Al_4Cu_9 phase (gray regions), together with a large number of pores. The SEM micrograph of the Cu–12Al–6Ni alloy is shown in Fig. 9, and the composition of each phase obtained by EDS analysis is listed in

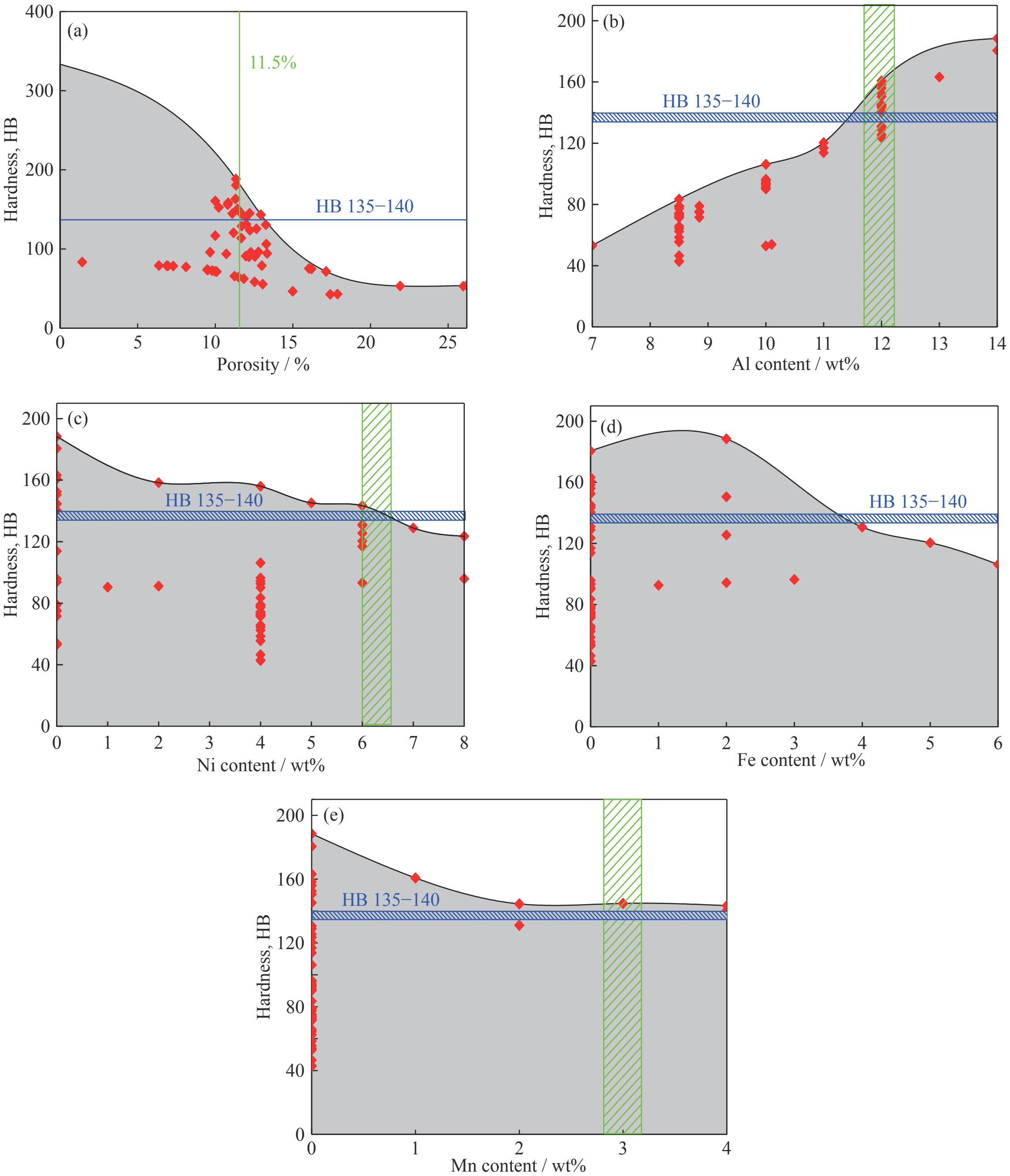

Fig. 6. Hardness distribution of the alloy with respect to its porosity and composition obtained using SMOreg/puk model: (a) porosity; (b) Al content; (c) Ni content; (d) Fe content; (e) Mn content.

Table 3. A large number of granular NiAl phases precipitated at the boundary between the α-Cu phase and the Al_4Cu_9 phase or within the α-Cu phase, whereas the morphology of the Al_4Cu_9 phase shows an irregular shape. Fig. 10 shows the XRD pattern of the alloy, the XRD results are in good agreement with the EDS analysis results.

According to the literature [49], the Cu–12Al–*x*Ni vertical section was drawn and presented in Fig. 11. The α-Cu phase was first precipitated at the boundary of β-$AlCu_3$ during cooling. When the temperature decreased to the eutectoid reaction for β-$AlCu_3$ → α-Cu + NiAl, this eutectoid reaction occurred. Because the NiAl phase was distributed in the grain boundary of the α-Cu phase, the growth of the α-Cu phase was effectively inhibited. When the temperature reached approximately 510°C, the second eutectoid reaction (β-$AlCu_3$ → α-Cu + NiAl + Al_4Cu_9) occurred. Because the first eutectoid reaction consumed a large amount of the β-$AlCu_3$ phase, the amount of products generated by the second

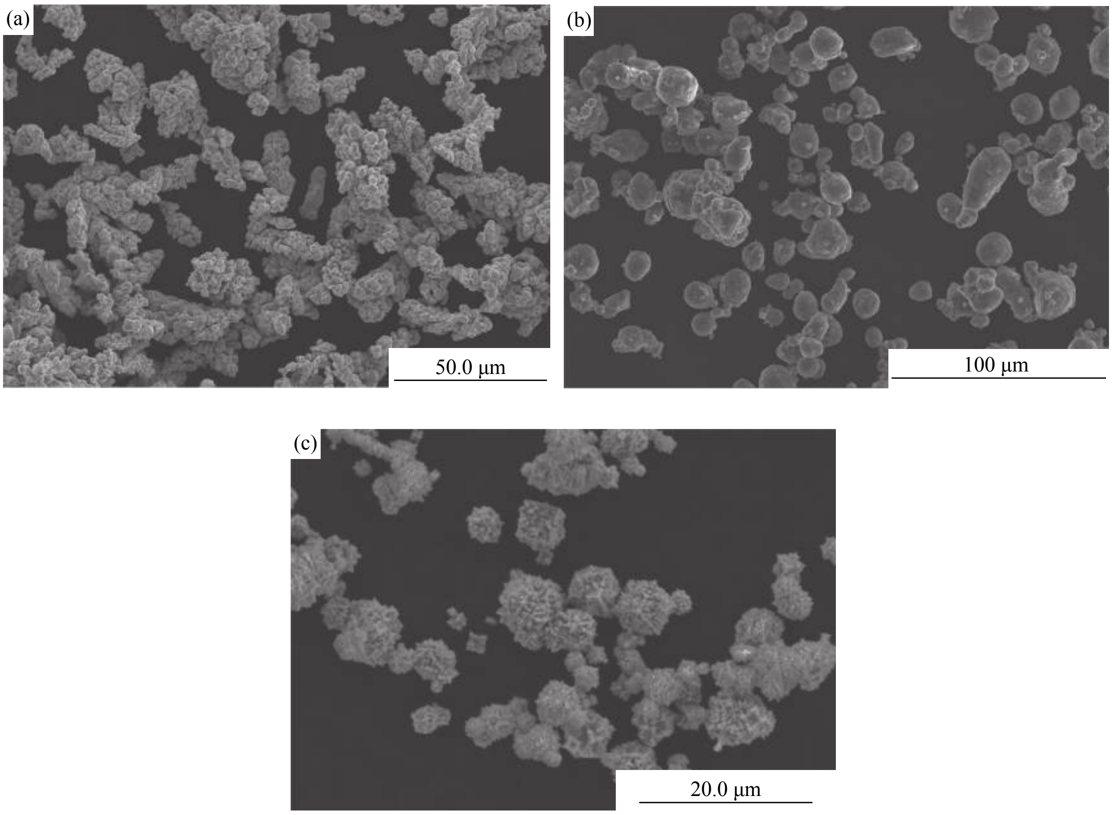

Fig. 7. Morphology of as-received powders: (a) Cu powder; (b) Al powder; (c) Ni powder.

Table 2. Characteristics of the experimental powders

Powder	Particle size distribution / μm			Purity / wt%	Method of Manufacture
	D_{10}	D_{50}	D_{90}		
Cu	12.8	23.8	42.7	99.9	Electrolytic
Al	10.6	17.8	28.9	99.7	Ar atomized
Ni	5.2	12.4	29.0	99.8	Carbonylation method

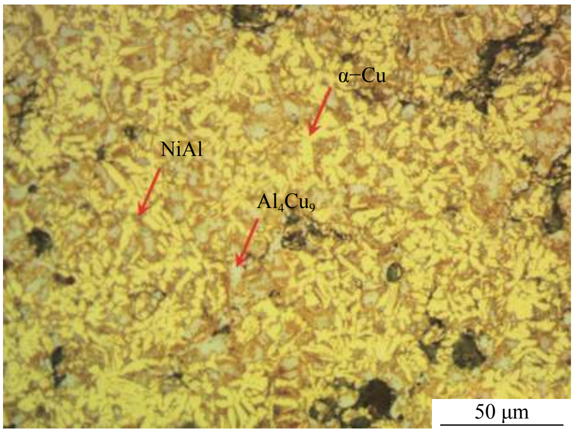

Fig. 8. Optical micrograph of the Cu–12Al–6Ni alloy.

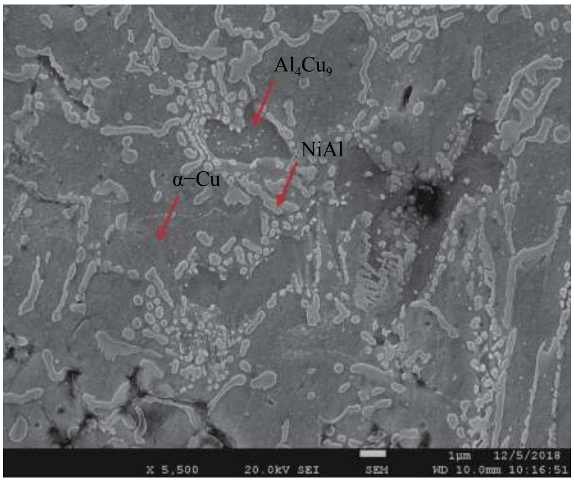

Fig. 9. SEM image of the Cu–12Al–6Ni alloy.

eutectoid was smaller, substantially decreasing the fraction of the Al_4Cu_9 phase. In the present work, the furnace cooling process was slow, therefore, no martensite phase was observed in the alloy.

The porosity, tensile strength, and hardness of the alloy are summarized in Fig. 12. The porosity of the sintered samples is 11.22%, which is 0.28% less than the target value.

Table 3. EDS analysis for each phase of Cu–12Al–6Ni alloy shown in Fig. 9 at%

Phase	Cu	Al	Ni
α-Cu	79.72	19.03	1.25
NiAl	12.01	45.52	42.47
Al_4Cu_9	61.28	32.22	6.50

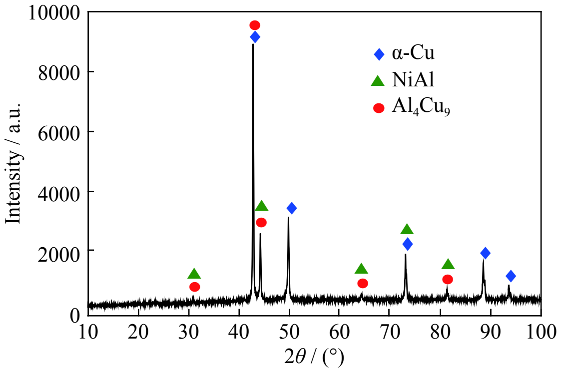

Fig. 10. XRD pattern of the Cu–12Al–6Ni alloy.

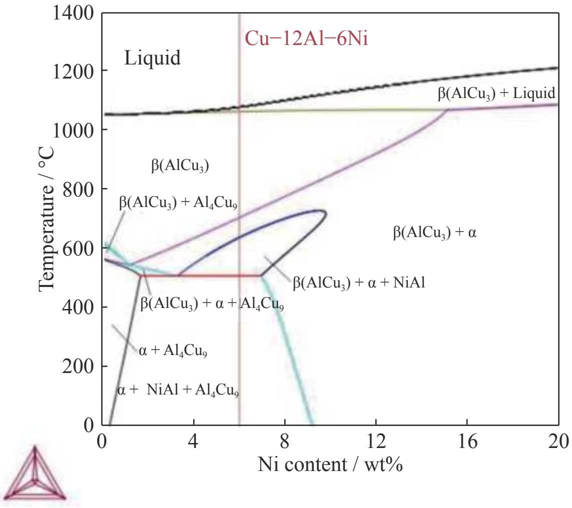

Fig. 11. Vertical section of the Cu–12Al–*x*Ni alloy according to the literature [49].

The tensile strength is about 390 MPa, which is 40 MPa greater than the target value and 10 MPa greater than the value predicted by the SMOreg/puk model. The hardness is about HB 139, which is HB 1 greater than the value predicted by the SMOreg/puk model. Therefore, the experimental values reached the target values. The refinement of the α-Cu phase in the alloy resulted in fine grain strengthening. Moreover, a large number of granular NiAl phases were dispersed in the alloy (NiAl is an intermetallic compound with high strength and microhardness), hence, the strength of the alloy was further improved.

The aforementioned results show that the SMOreg/puk model can well predict the properties of Cu–Al alloys and effectively guide the composition design of materials. Because the SMO algorithm has the advantages of fast training and strong generalization performance, it is widely used to predict the mechanical properties of structural materials [50]. The mapping capabilities of the puk kernel is stronger than that of other kernel functions, therefore, it can handle various mapping problems well. Moreover, the puk kernel can improve the generalization performance of the SMO algorithm [51].

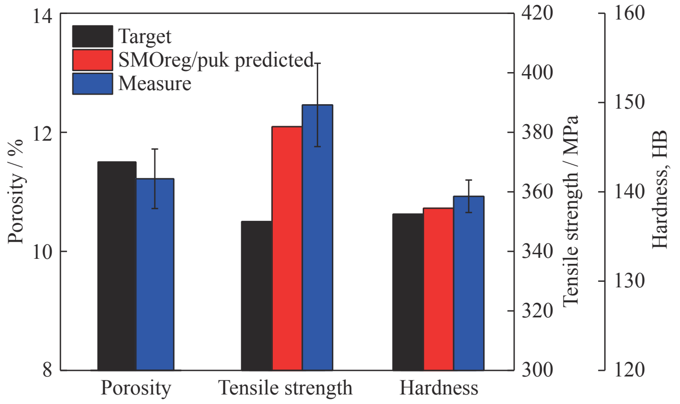

Fig. 12. Porosity, tensile strength, and hardness of the Cu–12Al–6Ni alloy.

6. Conclusions

In this study, the machine-learning approach was used to predict the tensile strength and hardness of Cu–Al alloys and provide guidance for composition design to achieve the expected values. Chemical composition and porosity were chosen as the descriptors, and six algorithms were used to build prediction models. The dataset used in this work were collected from experiments and the literature. The main conclusions are summarized as follows:

(1) The SMOreg/puk model showed the best performance, with the highest correlation coefficient and lowest er-

ror among the six investigated models. The tensile strength and hardness predicted by the SMOreg/puk model agree well with the experimental data, and the errors are less than 30.49 MPa and HB 8.6, respectively.

(2) According to the target values (a porosity of approximately 11.5%, tensile strength greater than 350 MPa, and hardness of HB 135–140), the chemical composition of Cu with 12wt% Al and 6wt% Ni alloy was obtained from the prediction by the SMOreg/puk model. The alloy was then prepared using the powder metallurgy method, and a porosity of 11.22%, a tensile strength of 390 MPa, and hardness of HB 139 were obtained. These parameters reached their expected values.

Acknowledgment

The authors acknowledge financial support from the National Key Research and Development Program of China (No. 2016YFB0700503), the National High Technology Research and Development Program of China (No. 2015AA03420), Beijing Science and Technology Plan (No. D16110300240000), National Natural Science Foundation of China (No. 51172018), and the Science and Technology Research Program of Chongqing Municipal Education Commission (No. KJQN201801202).

References

[1] J.L. Liu, H.Y. Huang, and J.X. Xie, Effects of aging treatment on the microstructure and superelasticity of columnar-grained $Cu_{71}Al_{18}Mn_{11}$ shape memory alloy, *Int. J. Miner. Metall. Mater.*, 23(2016), No. 10, p. 1157.

[2] M. Izadinia and K. Dehghani, Microstructural evolution and mechanical properties of nanostructured Cu–Al–Ni shape memory alloys, *Int. J. Miner. Metall. Mater.*, 19(2012), No. 4, p. 333.

[3] A. Sata and B. Ravi, Comparison of some neural network and multivariate regression for predicting mechanical properties of investment casting, *J. Mater. Eng. Perform.*, 23(2014), No. 8, p. 2953.

[4] N. Altinkok and R. Koker, Neural network approach to prediction of bending strength and hardening behaviour of particulate reinforced (Al–Si–Mg)–aluminium matrix composites, *Mater. Des.*, 25(2004), No. 7, p. 595.

[5] B. Zhao, T.Y. Yu, W.F. Ding, X.Y. Li, and H.H. Su, BP neural network based flexural strength prediction of open-porous Cu–Sn–Ti composites, *Prog. Nat. Sci.*, 28(2018), No. 3, p. 315.

[6] J.L. Tang, C.Z. Cai, S.J. Huang, and T.T. Xiao, Strength prediction for Al–Cu–Mg–Ag alloy based on support vector regression, *J. Aeronaut. Mater.*, 32(2012), No. 5, p. 92.

[7] G.X. Liu, L.N. Jia, B. Kong, S.B. Feng, H.R. Zhang, and H. Zhang, Artificial neural network application to microstructure design of Nb–Si alloy to improve ultimate tensile strength, *Mater. Sci. Eng. A*, 707(2017), p. 452.

[8] X.W. Yang, J.C. Zhu, Z.S. Nong, D. He, Z.H. Lai, Y. Liu, and F.W. Liu, Prediction of mechanical properties of A357 alloy using artificial neural network, *Trans. Nonferrous Met. Soc. China*, 23(2013), No. 3, p. 788.

[9] S.A. Razavi, F. Ashrafizadeh, and S. Fooladi, Prediction of age hardening parameters for 17-4PH stainless steel by artificial neural network and genetic algorithm, *Mater. Sci. Eng. A*, 675(2016), p. 147.

[10] D. Wu, W.L. Wang, L.G. Zhang, Z.Y. Wang, K.C. Zhou, and L.B. Liu, New high-strength Ti–Al–V–Mo alloy: from high-throughput composition design to mechanical properties, *Int. J. Miner. Metall. Mater.*, 26(2019), No. 9, p. 1151.

[11] Y.T. Lv, L.Q. Wang, J.W. Mao, and W.J. Lu, Recent advances of nickel–aluminum bronze (NAB), *Rare Met. Mater. Eng.*, 45(2016), No. 3, p. 815.

[12] Z.H. Deng, H.Q. Yin, X. Jiang, C. Zhang, K.Q. Zhang, T. Zhang, B. Xu, Q.J. Zheng, and X.H. Qu, Machine leaning aided study of sintered density in Cu–Al alloy, *Comput. Mater. Sci.*, 155(2018), p. 48.

[13] H. Wan, N.C. Si, G.L. Liu, M. Li, C. Xu, and L. Xu, Effect of rare earth on abrasion resistance of multi-aluminum bronze, *Chin. Rare Earths*, 36(2015), No. 4, p. 81.

[14] Y.Y. Li, W. Xia, W. Zhang, and Z.Q. Luo, Strong and wear resistant aluminum bronze alloy and its tribological characteristics, *Chin. J. Nonferrous Met.*, 6(1996), No. 3, p. 76.

[15] B.B. Lahiri, A. Sarkar, S. Bagavathiappan, A. Nagesha, T. Saravanan, R. Sandhya, T. Jayakumar, and J. Philip, Studies on temperature evolution during fatigue cycling of Ni–Al bronze (NAB) alloy using infrared thermography, *Insight: Non-Destr. Test. Cond. Monit.*, 58(2016), No. 2, p. 70.

[16] B. Zhang, X.J. Xu, S.D. Chen, and W. Jiang, Effects of zirconium and strontium on microstructure and properties of nickel aluminium bronze ingot, *Trans. Mater. Heat Treat.*, 36(2015), No. 3, p. 62.

[17] J.M. Ji, Y.Y. Lu, J. Wu, and G.C. Meng, Microstructure and wear resistance of new aluminum bronze with Ce, *Spec. Cast. Nonferrous Alloys*, 33(2013), No. 7, p. 672.

[18] Z.L. Guo, W.X. Tang, H.L. Zhang, J. Xu, and G. He, Influences of alloying elements on the properties of nickel aluminum bronzes, *Dev. Appl. Mater.*, 18(2003), No. 2, p. 39.

[19] B. Thossatheppitak, S. Suranuntchai, V. Uthaisangsuk, A. Manonukul, and P. Mungsuntisuk, Mechanical properties at high temperatures and microstructures of a nickel aluminum bronze alloy, *Adv. Mater. Res.*, 683(2013), p. 82.

[20] J. Anantapong, V. Uthaisangsuk, S. Suranuntchai, and A. Manonukul, Effect of hot working on microstructure evolution of as-cast nickel aluminum bronze alloy, *Mater. Des.*, 60(2014), p. 233.

[21] A.L. Dai, G.C. Yan, Z.Y. Zhu, and J.S. Liu, Effect of aluminum content on microstructure and properties of casting $CuAl_xFe_3$, *Nonferrous Met. Eng.*, 3(2013), No. 4, p. 22.

[22] J.H. Wang, X.X. Jiang, and S.Z. Li, Microstructure and properties of boron–aluminum bronze, *Acta Metall. Sin.*,

32(1996), No. 10, p. 1039.

[23] B.W. Wang, T. Wang, and Z.T. Wang, *Copper Alloy and Its Processing Technology*, Chemical Industry Press, Beijing, 2007, p. 45.

[24] Y.W. Li, L.R. Xiao, W. Zhang, X.J. Zhao, Y.F. Song, and L. Guo, Microstructure and mechanical properties of aluminum bronze with different Mn contents, *Chin. J. Rare Met.*, 41(2017), No. 9, p. 985.

[25] A.L. Dai, G.C. Yan, Z.Y. Zhu, K. Zhu, H. Chen, and W.M. Niu, Wear-friction behavior of novel high aluminum bronzes alloy Cu–12Al–X in high temperature condition, *Chin. J. Nonferrous Met.*, 23(2013), No. 11, p. 3083.

[26] W.S. Li, Z.P. Wang, Y. Lu, Y.H. Jin, L.H. Yuan, and F. Wang, Mechanical and tribological properties of a novel aluminum bronze material for drawing dies, *Wear*, 261(2006), No. 2, p. 155.

[27] Y.H. Jin, Y. Lu, Z.P. Wang, W S Li, and J.L. Xu, Anti-frictional characteristic of new complex Al–bronze Cu–14Al, *Spec. Cast. Nonferrous Alloys*, 24(2004), No. 3, p. 32.

[28] J.L. Xu, Z.P. Wang, C. Chen, and P.Q. La, Research into a new high-strength aluminium bronze alloy, *Int. J. Mater. Prod. Technol.*, 21(2004), No. 5, p. 443.

[29] Z. Li and C.G. Li, The preparation of abrasion-resistive, antifrietional complex aluminum bronze, *Shanghai Nonferrous Met.*, 14(1993), No. 6, p. 13.

[30] F. Liu, *Research on Microstructure and Processability of High Aluminium Bronze Alloy*[Dissertation], Jiangxi University of Science and Technology, Ganzhou, 2014, p. 24.

[31] M. Sadayappan, M. Sahoo, and H.T. Michels, Optimization of composition and mechanical properties of aluminum bronze alloy C95400, *Trans. Am. Foundry Soc.*, 112(2004), p. 509.

[32] A.Q. Wang, R. Xu, and C.Z. Chi, The friction characteristic and tensile properties of casting Al–bronze, *J. Liaoning Tech. Univ.* (*Nat. Sci. Ed.*), 19(2000), No. 1, p. 87.

[33] A.L. Dai, G.C. Yan, Z.Y. Zhu, and J.S. Liu, Effects of heating treatment on friction and wear properties of novel high aluminum bronze alloy, *Mater. Mech. Eng.*, 13(2013), No. 12, p. 333.

[34] C.X. Wang, C.H. Jiang, Z. Chai, M. Chen, L.B. Wang, and V. Ji, Estimation of microstructure and corrosion properties of peened nickel aluminum bronze, *Surf. Coat. Technol.*, 313(2017), p. 136.

[35] D.L. Hu, J.C. Cao, Z. Zhou, and S.Q. Zhang, Organism and properties of high-strength and wear-resistant bronze, *Nonferrous Met.*, 50(1998), No. 3, p. 99.

[36] Z.B. Qin, Q. Zhang, Q. Luo, Z. Wu, B. Shen, L. Liu, and W.B. Hu, Microstructure design to improve the corrosion and cavitation corrosion resistance of a nickel–aluminum bronze, *Corros. Sci.*, 139(2018), p. 255.

[37] M.E. Moussa, M.A. Waly, and M. Amin, Effect of high intensity ultrasonic treatment on microstructural modification and hardness of a nickel–aluminum bronze alloy, *J. Alloys Compd.*, 741(2018), p. 804.

[38] X.J. Xu, S.D. Chen, L. Pan, J. Wei, and G.F. Shi, Microstructure and properties of Zr microalloying nickel aluminum bronze ingot, *Chin. J. Rare Met.*, 38(2014), No. 1, p. 158.

[39] M. Yaşar and Y. Altunpak, The effect of aging heat treatment on the sliding wear behaviour of Cu–Al–Fe alloys, *Mater. Des.*, 30(2009), No. 3, p. 878.

[40] C.Z. Zhang, Q.X. Sun, and H.X. Zhang, Sintering mechanism of Cu–Al system powder billet, *J. Northeast Univ. Technol*, 10(1989), No. 5, p. 561.

[41] R. Wang, Y.P. Bao, Y.H. Li, Z.J. Yan, D.Z. Li, and Y. Kang, Influence of metallurgical processing parameters on defects in cold-rolled steel sheet caused by inclusions, *Int. J. Miner. Metall. Mater.*, 26(2019), No. 4, p. 440.

[42] L. Panda, P.K. Banerjee, S.K. Biswal, R. Venugopal, and N.R. Mandre, Artificial neural network approach to assess selective flocculation on hematite and kaolinite, *Int. J. Miner. Metall. Mater.*, 21(2014), No. 7, p. 637.

[43] K. Xu, Y.H. Ai, and X.Y. Wu, Application of multi-scale feature extraction to surface defect classification of hot-rolled steels, *Int. J. Miner. Metall. Mater.*, 20(2013), No. 1, p. 37.

[44] K.Q. Zhang, H.Q. Yin, X. Jiang, X.Q. Liu, F. He, Z.H. Deng, D.F. Khan, Q.J. Zheng, and X.H. Qu, A novel approach to predict green density by high-velocity compaction based on the materials informatics method, *Int. J. Miner. Metall. Mater.*, 26(2019), No. 2, p. 194.

[45] F.F. Yang, H.J. Kang, E.Y. Guo, R.G. Li, Z.N. Chen, Y.H. Zeng, and T.M. Wang, The role of nickel in mechanical performance and corrosion behaviour of nickel–aluminium bronze in 3.5wt% NaCl solution, *Corros. Sci.*, 139(2018), p. 333.

[46] Q.F. Kang, S.B. Hu, S.Q. Zeng, and G.K. Chen, Heat treatment strengthening of nickel–aluminum bronze alloy for marine propeller, *Chin. J. Nonferrous Met.*, 28(2018), No. 1, p. 107.

[47] G.Q. Tian, Y. Lu, K. Lu, and W.S. Li, Influence of Co on the wear behavior of high-aluminum bronze, *Rare Met. Mater. Eng.*, 27(2008), No. 10, p. 1833.

[48] S.S. Rathore and V.V. Dabhade, Dimensional change during sintering of Fe–Cu–C alloys: a comparative study, *Trans. Indian Inst. Met.*, 69(2016), No. 5, p. 991.

[49] J. Miettinen, Thermodynamic description of the Cu–Al–Ni system at the Cu–Ni side, *Calphad*, 29(2005), No. 1, p. 40.

[50] Y.L. Lin, J.G. Hsieh, H.K. Wu, and J.H. Jeng, Three-parameter sequential minimal optimization for support vector machines, *Neurocomputing*, 74(2011), No. 17, p. 3467.

[51] B. Üstün, W.J. Melssen, and L.M.C. Buydens, Facilitating the application of support vector regression by using a universal pearson VII function based kernel, *Chemom. Intell. Lab. Syst.*, 81(2006), No. 1, p. 29.